Heliyon

Received:
7 January 2019
Revised:
4 March 2019
Accepted:
25 March 2019

Cite as: V. I. Popkov, V. P. Tolstoy, V. N. Nevedomskiy. Peroxide route to the synthesis of ultrafine CeO_2-Fe_2O_3 nanocomposite via successive ionic layer deposition. Heliyon 5 (2019) e01443. doi: 10.1016/j.heliyon.2019.e01443

Peroxide route to the synthesis of ultrafine CeO_2-Fe_2O_3 nanocomposite via successive ionic layer deposition

V. I. Popkov [a,b,c,*], **V. P. Tolstoy** [a], **V. N. Nevedomskiy** [b]

[a] *Institute of Chemistry, Saint Petersburg State University, 26 Universitetskii Prospect, Petergof, St. Petersburg, 198504, Russian Federation*

[b] *Ioffe Institute, 26 Politekhnicheskaya Street, St. Petersburg, 194021, Russian Federation*

[c] *Saint-Petersburg State Institute of Technology, 26 Moskovsky Prospect, St. Petersburg, 190013, Russian Federation*

[*] Corresponding author.

E-mail address: vadim.i.popkov@gmail.com (V.I. Popkov).

Abstract

An ultrafine α-CeO_2—α-Fe_2O_3 nanocomposite was prepared from the ultradispersed nanoparticles of cerium (IV) and iron (III) amorphous hydroxides heat-treated at 600 °C and 900 °C in the air. The initial composites were obtained by the successive ionic layer deposition (SILD) method. According to scanning electron microscopy (SEM), energy dispersive X-ray spectroscopy (EDX) and powder X-ray diffraction (PXRD), the cerium/iron ratio in the synthesized nanocomposite is close to 1:2, and the α-CeO_2 and α-Fe_2O_3 nanocrystals are isometrically shaped and have an average size of 4 ± 1 and 7 ± 1 nm (600 °C) and 24 ± 2 and 35 ± 3 nm (900 °C), respectively. Transmission electron microscopy (TEM) and selected area electron diffraction (SAED) have shown that nanocrystals are evenly distributed in the composite volume and are spatially conjugated. The formation mechanisms of both initial amorphous composites of cerium (IV) and iron (III) hydroxides and of α-CeO_2 and α-Fe_2O_3 nanocrystals were established. It was shown that synthesis of the initial hydroxide composite using the SILD method proceeds via the formation of amorphous cerium hydroxo-peroxide ($CeO(OOH)_2$). As a result of the study, a

https://doi.org/10.1016/j.heliyon.2019.e01443

schematic mechanism for the formation of a composite based on ultrafine nanocrystals of cerium (IV) and iron (III) oxides has been proposed.

Keywords: Materials science, Nanotechnology, Physical chemistry, Materials chemistry, Inorganic chemistry

1. Introduction

The nanomaterials based on iron (III) and cerium (IV) oxides are currently in the focus of attention of numerous scientific groups because of their broad potential use. Such nanostructured oxides as cerium orthoferrite ($CeFeO_3$), cerium dioxide-based solid solutions ($CeO_2(Fe_2O_3)$) and CeO_2-Fe_2O_3 composite find application as photocatalytic materials [1, 2, 3]; as sorbents of anions of fluorine [4, 5], arsenic (III, V) [6, 7] and antimony (III, V) [8]; as basic materials for catalysts in carbon and soot oxidation [9], selective NO_x reduction [10], nitrobenzene ozonation [11] and methane reforming via chemical looping [12, 13, 14]. While the CeO_2/Fe_2O_3 ratio can vary over a wide range among the composite materials depending on their application, the functional properties of the nanostructured iron (III) and cerium (IV) oxides are clearly a function of the crystallite size. Since most of the above-mentioned applications are associated with the processes occurring on the surface of nanoparticles (NPs), of particular interest are the fine ($\leq$10 nm) CeO_2 and Fe_2O_3 nanocrystals with a narrow size distribution, high specific surface area and uniform distribution of iron (III) and cerium (IV) oxides throughout the composite volume [15, 16]. The latter circumstance is especially important for the chemical looping processes, since the close location and spatial conjunction of the components promote oxygen vacancies generation by means of CeO_2 partial reduction and fast oxygen transfer through the vacancies from the oxygen carrier, i.e., Fe_2O_3 nanoparticles [17, 18].

However, it is a challenge to synthesize nanocomposites based on CeO_2 and Fe_2O_3 crystals sized below 10 nm and to achieve their uniform distribution in the volume. This is due to a great difference in the chemical properties of the precursors used in the most common methods of nanoparticle synthesis, and to a difference between the temperatures of crystallization and those of the onset of iron (III) and cerium (IV) oxides active mass transfer. These circumstances seriously limit the use of conventional synthesis methods for obtaining the above-mentioned composite nanoparticles [19]. A review of the studies devoted to the problem of simultaneous synthesis of nanocrystalline oxides by the widely applied soft-chemistry methods (Table 1) shows that this problem can be solved only by using quite expensive precursors and complex synthesis techniques (see, e.g., [20]), but even in this case the minimal size of cerium/iron oxide nanoparticles is about 10–20 nm [21, 22, 23, 24]. Thus, a solution of this problem makes it necessary to perform synthesis in softer conditions than the already used ones.

https://doi.org/10.1016/j.heliyon.2019.e01443

Table 1. Morphology and the average size of CeO_2/Fe_2O_3 nanocrystals in composites obtained via various soft-chemistry methods.

Synthesis technique	Morphology of CFNPs	The average size of CFNPs, nm
Urea hydrolysis method [21]	rod-like	200
HT of polyol-based metal alkoxides [22]	hollow sphere	50
Hydrothermal synthesis [23]	spherical	35−40
Glycine-nitrate combustion [24]	foam-like	12−32
HT of co-precipitated carbonates [2]	close to isometric	10−20
Nanoprecipitation in a basic media [20]	isometric	8−11
HT of hydroxide NPs synthesized via SILD [this work]	spherical	4−7

Abbreviation: CFNPs − CeO_2-Fe_2O_3 nanoparticles, HT − heat treatment.

The successive ionic layer deposition (SILD) is a representative of the layer-by-layer nanomaterial synthesis, which takes place on the substrate surface due to the sequential interaction of components of the reacting solutions, can be considered as a method that provides conditions described above [25]. In this case, the formation reactions take place at room temperature and ensure the obtaining of fine nanoparticles and composites on their basis. Feasibility of using this method for obtaining nanostructured hydroxide derivatives of d- and f-metals with different structure and composition was demonstrated in [26, 27, 28, 29]. As a rule, the synthesized products are represented by hydroxides and other low-temperature derivatives of the corresponding elements and an additional thermal treatment in the air is required to obtain CeO_2-Fe_2O_3 nanocomposite by this method [30].

Therefore, the present research was aimed at developing a technique for synthesizing a composite based on fine CeO_2 and Fe_2O_3 nanocrystals by the SILD method that provides a narrow size distribution of the nanocrystals and high homogeneity of the composite. At the same time, mechanisms of formation of iron (III) and cerium (IV) amorphous hydroxide nanoparticles under the SILD conditions and their evolution into nanocrystalline CeO_2 and Fe_2O_3 oxides under thermal treatment in the air were studied. A thorough physicochemical investigation of these processes resulted in establishing regularities of the CeO_2-Fe_2O_3 nanocomposite formation and suggested a schematic representation of the formation mechanism.

2. Experimental

2.1. Synthesis of CeO_2-Fe_2O_3 nanocrystals via SILD

The single-crystal silicon wafers with <100 > orientation and a size of 10 × 20 × 0.35 mm were used as a substrate for the synthesis and physicochemical

https://doi.org/10.1016/j.heliyon.2019.e01443

characterization. The silicon wafer was cleaned for 10 minutes in an ultrasonic bath filled with acetone. Then, the plate was sequentially treated for 10 minutes in concentrated HF, washed with deionized water several times, then placed into 0.1M KOH solution and again washed with water.

For the synthesis of initial hydroxide nanoparticles, different aqueous solutions or distilled water were used according to the synthesis scheme presented in Fig. 1:

I – aqueous solution of 0.01M $Ce(NO_3)_3$ and 0.01M $(NH_4)_2Fe(SO_4)_2$ (Mohr's salt);

II – distilled water;

III – aqueous solution of H_2O_2 (3% mass.) with the addition of KOH to pH = 10;

IV – distilled water.

As the first step of the SILD synthesis procedure, the substrate Si plate was immersed into solution I and after that the excess reagent was washed from it with distilled water (II). As the second step, the plate was immersed in solution III and again washed in distilled water (IV). This sequence corresponds to one SILD cycle, which is repeated 30 times to obtain the desired thickness of the hydroxide nanoparticle layer. The time of treatment in reagent solutions and of washing in water was 30 s. A more detailed description of the method of hydroxide nanocomposites synthesis by the peroxide route of SILD is given in [26]. Finally, the synthesized hydroxide nanoparticles were calcined at 600 and 900 °C for 1 hour to obtain the CeO_2-Fe_2O_3 nanoparticles.

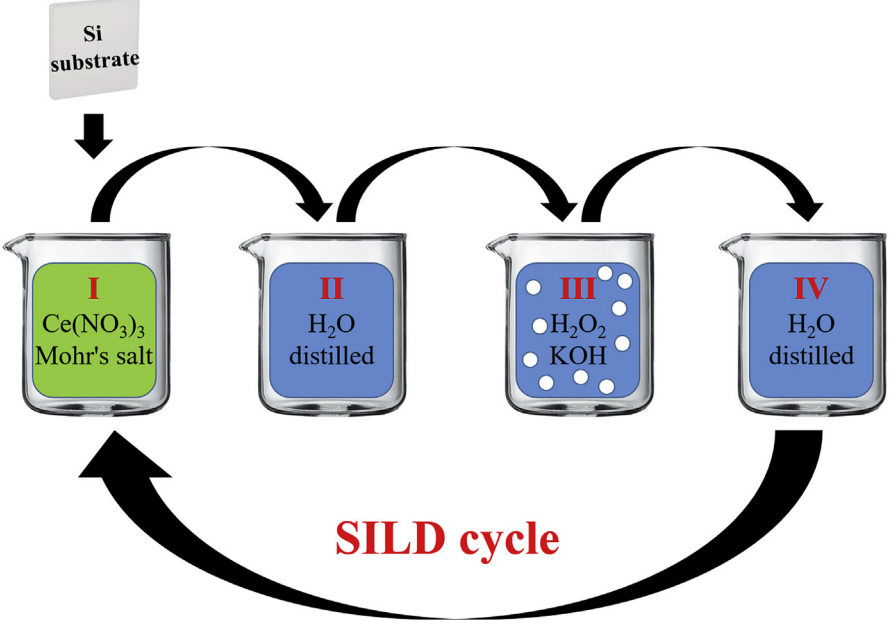

Fig. 1. Synthesis of initial cerium/iron hydroxide nanoparticles via SILD technique.

https://doi.org/10.1016/j.heliyon.2019.e01443

2.2. Physicochemical characterization of CeO_2-Fe_2O_3 nanocrystals

The morphology and composition of the samples were examined by scanning electron microscopy (Tescan Vega 3 SBH SEM) and by energy-dispersive X-ray spectroscopy (EDX) using the Oxford INCA 200 detector. ImageJ software was used for determining nanoparticle size from the SEM images. Powder X-ray diffraction (PXRD) patterns were recorded using the Rigaku SmartLab 3 diffractometer with Cu Kα1 emission (0.154056 nm). JEOL TEM-100CX was applied to evaluate morphology and microstructure of the prepared samples by transmission electron microscopy (TEM) as well as to gather information about the sample phase composition by means of selected area electron diffraction (SAED). The structural characterization was carried out by using Raman spectroscopy (SINTERRA Raman microscope) with a laser ($\lambda = 532$ nm). The thermal behavior of the sample was investigated by the simultaneous thermogravimetric and differential thermal analysis (DTA-TG) by using Shimadzu DTG-60.

3. Results and discussion

As a result of successive 30 cycles of SILD, a smooth brown film was obtained on the surface of the Si substrate. The processes involved can be approximately described by the following chemical Eqs. (1) and (2):

$$2Ce(NO_3)_3 + 6KOH + 5H_2O_2 = 2CeO(OH)_2\downarrow + 6KNO_3 + 6H_2O \quad (1)$$

$$2(NH_4)_2Fe(SO_4)_2 + 4KOH + H_2O_2 = 2FeOOH\downarrow + 2(NH_4)_2SO_4 + 2K_2SO_4 + 2H_2O \quad (2)$$

According to the EDX data (Fig. 2a), the cerium/iron ratio in the sample is 35.2%:64.8%, that is, about 1:2. Also it should be noticed that the sample includes a small potassium impurity, the atomic fraction of which does not exceed 3%. The SEM examination of the film (Fig. 2b) has found that it is composed of isometric nanoparticles with an average size about 10 nm. This composition retains its morphological structure after heat treatment, however, there was a noticeable increase in particle size along with the temperature increase up to 600 °C (Fig. 2c) and further to 900 °C (Fig. 2b).

The XRD pattern (Fig. 3) demonstrates only an amorphous halo in the 25−30° range of Bragg angles, which clearly suggests the amorphous nature of the nanoparticles. Thus, the application of the SILD method resulted in synthesizing amorphous fine nanoparticles based on hydroxide derivatives of cerium and iron, which formed

https://doi.org/10.1016/j.heliyon.2019.e01443

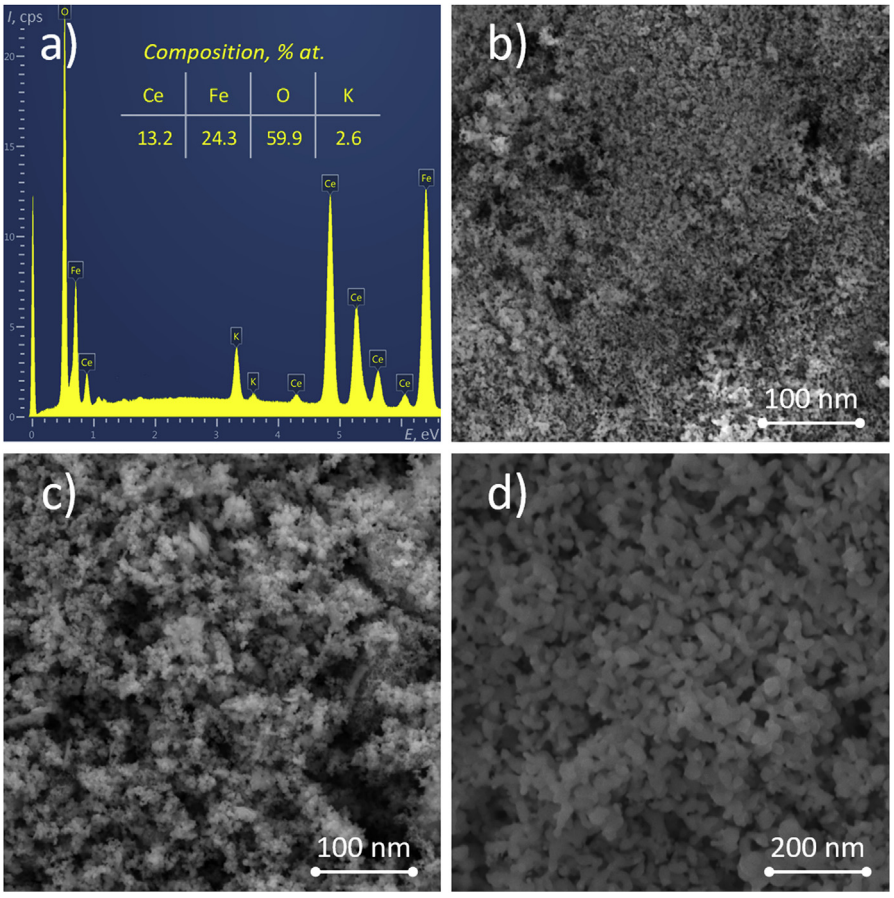

Fig. 2. EDX spectra (a) and SEM micrographs (b) of initial hydroxide NPs and SEM micrographs of CFNPs obtained via heat treatment at 600 °C (c) and 900 °C (d).

through precipitation of corresponding cations in an alkaline KOH solution and further were used as precursors for oxide nanocrystals preparation. After heat treatment at 600 and 900 °C, formation of the nanocrystalline oxides of cerium (IV) and iron (III) with a structure of α-CeO_2 and α-Fe_2O_3 occurred (Fig. 3b and c, respectively). A more detailed description of the diffraction results of these samples is given below.

To determine the temperature of nanocrystal formation, the simultaneous thermal analysis (DTA-TG) of the amorphous nanoparticles was done. Its results presented in Fig. 4 indicate that the hydroxide precursor decomposition is followed by a number of exothermic and endothermic effects, the major of which can be related to the following processes:

108 °C – an endothermic effect caused by the removal of physically adsorbed water

270 °C – an endothermic effect caused by the decomposition of oxide-hydroxide of iron (III):

https://doi.org/10.1016/j.heliyon.2019.e01443

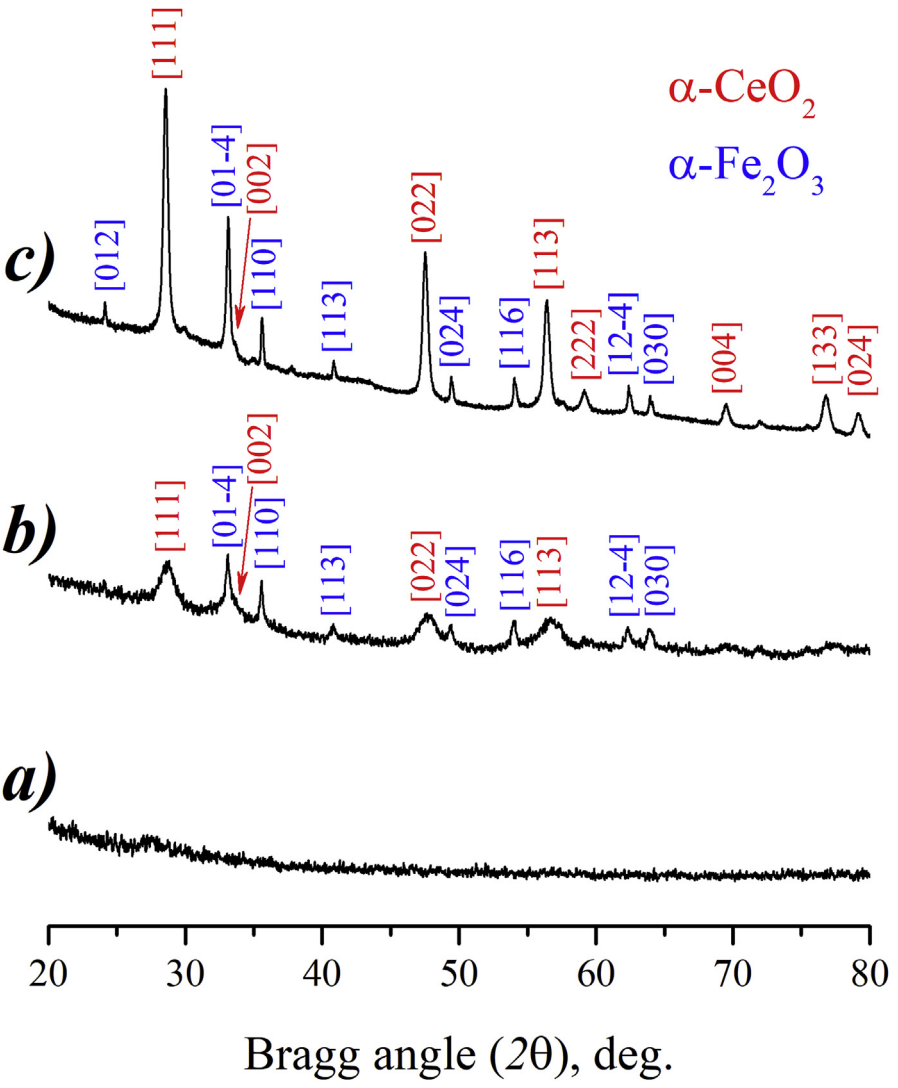

Fig. 3. PXRD patterns of initial hydroxide NPs and CFNPs obtained via its heat treatment at 600 °C and 900 °C.

$$2am\text{-}FeOOH \rightarrow am\text{-}Fe_2O_3 + H_2O \quad (3)$$

397 °C – an endothermic effect caused by the decomposition of peroxo-hydroxide of cerium (IV):

$$am\text{-}CeO(OOH)_2 \rightarrow am\text{-}CeO(OH)_2 + O_2 \quad (4)$$

430 °C – an endothermic effect caused by the decomposition of oxide-hydroxide of cerium (IV):

$$am\text{-}CeO(OH)_2 \rightarrow am\text{-}CeO_2 + H_2O \quad (5)$$

482 °C – an exothermic effect caused by cerium (IV) oxide crystallization:

https://doi.org/10.1016/j.heliyon.2019.e01443

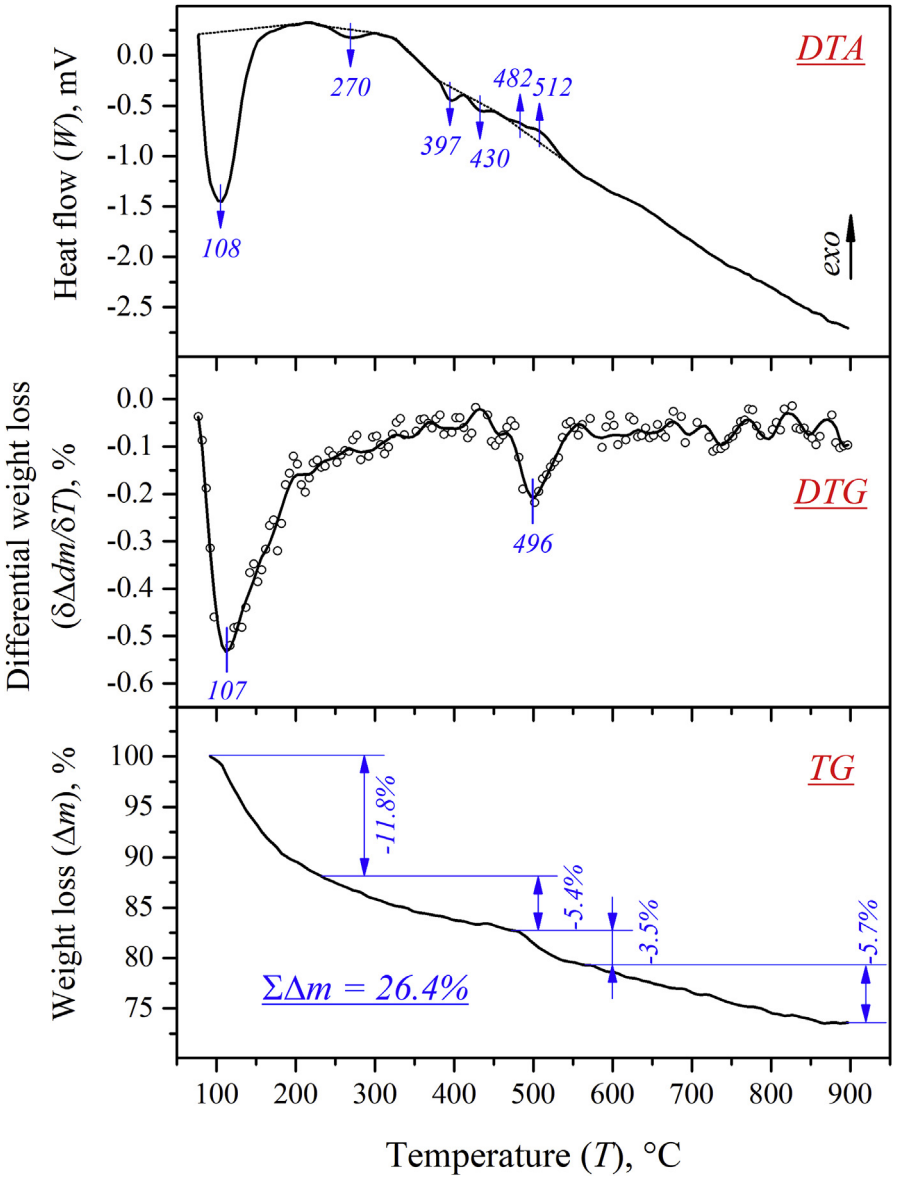

Fig. 4. DTA/TG/DTG curves of initial hydroxide NPs.

$$am\text{-}CeO_2 \rightarrow \alpha\text{-}CeO_2 \quad (6)$$

512 °C – an exothermic effect caused by iron (III) oxide crystallization:

$$am\text{-}Fe_2O_3 \rightarrow \alpha\text{-}Fe_2O_3 \quad (7)$$

The described effects are accompanied by a considerable mass loss, which mainly is due to the removal of adsorbed water (-11.8%), removal of water resulting from iron (III) oxide-hydroxide decomposition (-5.4%), removal of oxygen resulting from cerium peroxo-hydroxide decomposition (3.5%), and also due to the kinetically

https://doi.org/10.1016/j.heliyon.2019.e01443

hindered removal of water and carbon dioxide adsorbed on the nanoparticle surface (-5.7%). The greatest mass loss is observed at 107 and 496 °C, as it follows from the differential thermogravimetric analysis (DTG) curve, and can be attributed to the above described hydroxide precursors decomposition. However, a discrepancy between the thermal effect (430 °C) and the mass loss effects (497 °C) was observed. Apparently, a delayed effect of mass loss is observed in this case due to the kinetic difficulties in water removal after its formation in the hydroxide. That is, at a given rate of change in the measured temperature (10°/min), the removal of water from the sample lags by 4−5 minutes with respect to the decomposition reaction. Kinetic difficulties may arise due to the shielding of the inner layers of hydroxide nanoparticles by the outer ones.

Thus, the minimum temperature of cerium (IV) and iron (III) oxides formation is 600 °C, and the complete removal of by-products from the hydroxide precursor heat treatment ends up at 900 °C. Therefore, these temperatures were chosen for the further investigation aimed at the synthesis of nanocrystalline cerium (IV) and iron (III) oxides.

The hydroxide precursor nanoparticles were treated at 600 and 900 °C for 1 hour in the air. The samples' XRD patterns obtained after the heat treatments are presented in Fig. 3. According to these data, nanocrystalline cerium (IV) and iron (III) oxides with a structure of α-CeO_2 and α-Fe_2O_3 become fully formed at both 600 and 900 °C (Fig. 3, b and c, respectively), and the average size calculated from the line broadening is 4 ± 1 and 7 ± 1 nm at 600 °C, 24 ± 2 and 35 ± 3 nm at 900 °C, respectively. The crystalline phases ratio determined by quantitative phase analysis and expressed as CeO_2:$FeO_{1.5}$, is 36.8%:63.2% (600 °C) and 36.7%:63.3% (900 °C), and corresponds to the EDX data within the margin of error. Due to the match of EDX and PXRD results, one can assume that cerium (IV) and iron (III) oxides prepared by heat treatment of amorphous hydroxide nanoparticles primarily exist within the composite as α-CeO_2 and α-Fe_2O_3. Along with that, according to the SEM images (Fig. 2, c−d), morphological peculiarities of α-CeO_2 and α-Fe_2O_3 nanoparticles remain the same as they were before the heat treatment, that is, the nanoparticles retain spherical shape, but their average size increases noticeably, especially in the sample prepared at 900 °C (Fig. 2, d).

To determine the positional relationship of CeO_2 and α-Fe_2O_3 nanocrystals within the composite prepared by the hydroxide precursor heat treatment at 600 °C, TEM and SAED studies were carried out (Fig. 5). According to a comparison of the TEM data measured in the bright-field and dark-field modes (Fig. 5, a, and b, respectively), CeO_2 and α-Fe_2O_3 nanocrystals are evenly arranged within the entire volume of the sample. The diffraction ring positions in SAED patterns of the nanocomposite (Fig. 5, c) match the known interplanar distances in α-CeO_2 and α-Fe_2O_3, and confirm it that individual nanocrystals observed in the dark-field mode (Fig. 5, b)

https://doi.org/10.1016/j.heliyon.2019.e01443

correspond to cerium (IV) and iron (III) oxides. The TEM images of high magnification and high resolution demonstrated that both α-CeO_2 and α-Fe_2O_3 nanocrystals are spherical in shape and have similar size about 5−7 nm. Moreover, interplanar distances found by microscopy for the nanocrystals of cerium (IV) and iron (III) oxides along (111) and (110) crystallographic directions, accordingly, are 0.32 and 0.26 nm and correspond to the values found by XRD (0.311 and 0.252 nm).

Thus, it was shown for the first time that the synthesis of a composite based on fine α-CeO_2 and α-Fe_2O_3 nanocrystals with an average size of 5−7 nm (by both PXRD and TEM methods) can be achieved via SILD synthesis of amorphous nanoparticles of cerium and iron hydroxide derivatives followed by their heat treatment in the air. However, the nature of the formation of nanoparticles based on cerium (IV) and iron (III) hydroxides still remains not clear. In order to define the mechanism of their formation, the samples obtained at stage III of the 29th cycle and stage I of the 30th cycle (in accordance with the captions in Fig. 1) were investigated by Raman spectroscopy. A comparison of Raman spectra (Fig. 6) of the Si substrate obtained by its successive dipping at first into the 3% H_2O_2 solution for 30 sec and then into the $Ce(NO_3)_3$ and Mohr's salt solution has shown that besides the Fe-O stretching vibrations (221 and 287 cm^{-1}) in iron (III) oxide-hydroxide [31, 32] and Ce-O stretching vibrations (402 and 490 cm^{-1}) in cerium (II) oxide-hydroxide [17, 33], the mode at 830 cm^{-1} attributed to the stretching vibrations of Ce-O_2- peroxide group [34] was present in the spectrum in the first case and was absent in the second one.

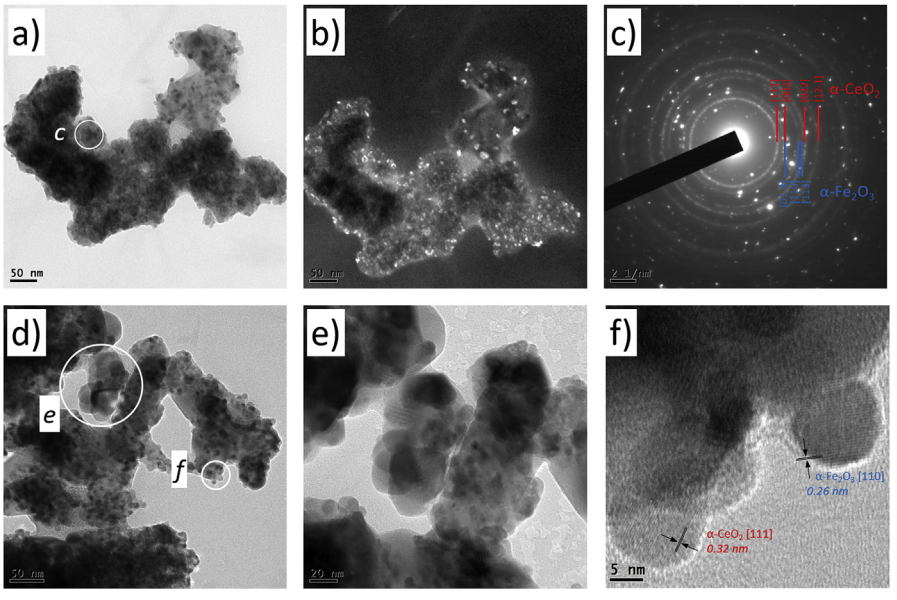

Fig. 5. The bright-field (a, d, e) and dark-field (b) transmission electron microscopy (TEM) image of CeO_2/Fe_2O_3 nanoparticles, its corresponding high resolution-TEM (HR-TEM) image (f) and selected area electron diffraction (SAED) pattern (c).

https://doi.org/10.1016/j.heliyon.2019.e01443

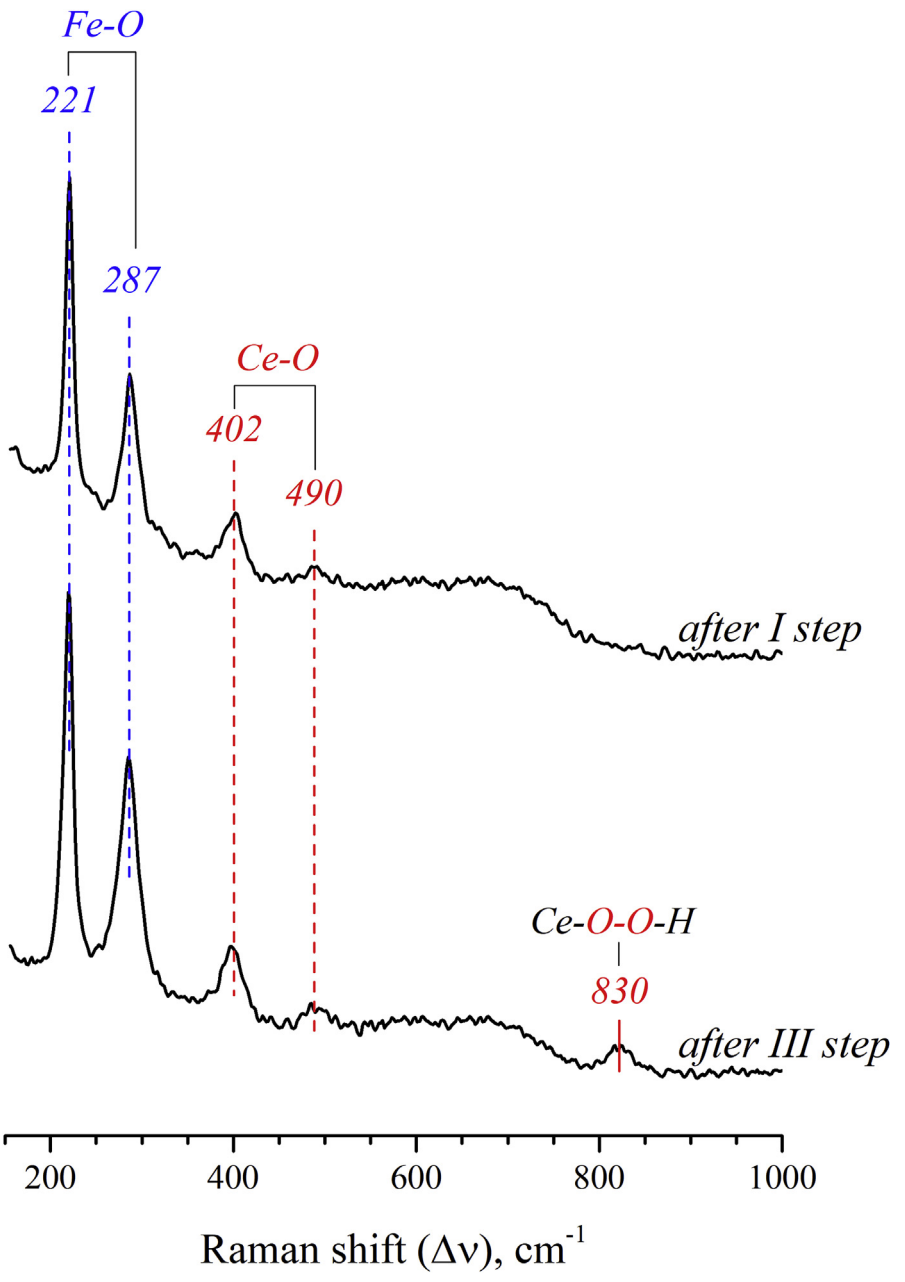

Fig. 6. Raman spectra of the initial film of hydroxide NPs synthesized via SILD at III step of the 29-th cycle and I step of the 30-th cycle.

These findings confirm that one of the intermediate products formed at stage III of the SILD cycle is $CeO(OOH)_2$, but being an unstable chemical compound after dipping into the solution of cerium (III) and iron (II) salts, it undergoes decomposition according to the following equation:

$$CeO(OOH)_2 \rightarrow CeO(OH)_2 + O_2 \quad (8)$$

and cerium (III) and iron (II) ions apparently catalyze this process [35, 36].

https://doi.org/10.1016/j.heliyon.2019.e01443

Since the results of a simultaneous thermal analysis demonstrate the presence of an effect associated with the decomposition of cerium hydroxo-peroxide at 397 °C [37, 38] according to Eq. (4), it may be supposed that the compound remains in the sample after synthesis, and that the process of its decomposition in solution III occurs predominantly on the surface of the particles due to diffusion limitations preventing its occurrence in the nanoparticles bulk, as was shown, for example, in [39]. Besides, based on the mass losses in the processes of am-CeO(OOH)2 and am-CeO(OH)2 decomposition (Fig. 4), the masses of am-CeO(OOH)2 and am-CeO(OH)2 were assessed to equal 2.43 mg and 18.47 mg, respectively. It follows from a consideration of a composite particle with a core of am-CeO(OH)2 and a shell of am-CeO(OOH)2, with an overall size of 10 nm (the average size of the obtained hydroxide nanoparticles), that the core diameter is 9.6 nm and the shell thickness is 0.2 nm. Thus, an assumption about the near-surface location of cerium hydroxo-peroxide is indirectly confirmed.

Based on the above, it was established that the formation of $CeO(OOH)_2$ by SILD technology is one of the key factors ensuring the «layer-by-layer » mode in the formation of the nanoparticles based on cerium (IV) and iron (III) hydroxides, which are similar in size and are spatially conjugated within the volume of the composite. This, in its turn, opens up a possibility to produce composites based on α-CeO_2 and α-Fe_2O_3 nanocrystals inheriting peculiarities of the morphology and spatial arrangement of the initial precursor.

The obtained results made it possible to schematically present the suggested mechanisms of amorphous hydroxide nanoparticles formation by SILD technology, and of a composite based on α-CeO_2 and α-Fe_2O_3 fine oxide nanocrystals under heat treatment in the air (Fig. 7). According to the proposed scheme, the Si substrate dipping into the cerium (III) and iron (II) salts solution entails adsorption of Fe^{2+} and Ce^{3+} hydrated ions on the substrate surface, which is negatively charged due to the sample preparation (see the Experimental section). After that, the excess reagents are washed off with distilled water (stage II of SILD cycle) and the substrate with the adsorbed ions is placed into 3% H_2O_2 solution (stage III of SILD cycle), where the processes described above take place and formation of the FeOOH and $CeO(OOH)_2$ phases occurs. FeOOH and $CeO(OOH)_2$ form a monolayer on the Si substrate surface. After the next washing with distilled water (stage IV of SILD cycle), the Si substrate with the adsorbate is dipped into the solution of cerium (III) and iron (II) salts again. This was found to lead to the decomposition of cerium peroxo-hydroxide into oxide-hydroxide and the subsequent adsorption of hydrated Fe^{2+} and Ce^{3+} ions on the surface of FeOOH and $CeO(OH)_2$. After 30 iterations of this cycle and coating the Si substrate with the mentioned substances in «layer-by-layer » mode, there forms a bulk composite consisting of fine nanoparticles of amorphous FeOOH and $CeO(OH)_2$ hydroxides. Their further heat treatment at

https://doi.org/10.1016/j.heliyon.2019.e01443

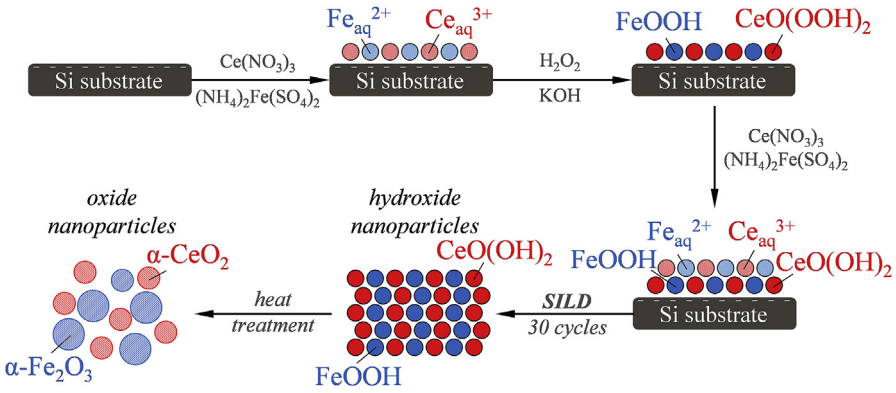

Fig. 7. Schematic representation of formation mechanism of nanocomposite of ultrafine cerium (IV) and iron (III) oxides synthesized via peroxide route of SILD.

600 °C and over results in the formation of a composite of α-CeO_2 and α-Fe_2O_3 nanocrystalls, the morphology and spatial arrangement of which remain mostly the same as in the precursor from nanoparticles of amorphous FeOOH and $CeO(OH)_2$. Thus, an approach based on the SILD synthesis of amorphous nanoparticles of cerium (IV) and iron (III) hydroxides followed by their heat treatment at a moderate temperature (600 °C) makes it possible to produce homogeneous composites from fine α-CeO_2 and α-Fe_2O_3 nanocrystals with an average size of 5−7 nm.

4. Conclusions

The present study suggests an original approach to the synthesis of nanoparticles of amorphous cerium (IV) and iron (III) hydroxides by the SILD method for the further production of the nanoparticle-based fine oxide nanocrystals via additional heat treatment. The mechanism of the amorphous hydroxide nanoparticles formation under SILD conditions was established. The formation of cerium peroxo-hydroxide ($CeO(OOH)_2$) as an intermediate product of «layer-by-layer » synthesis was studied. The mechanism of the formation of a nanocomposite based on fine nanocrystals of cerium (IV) and iron (III) oxides that emerge during the heat treatment of amorphous hydroxide nanoparticles was established. It was shown that the suggested route gives a possibility to produce composites from α-Fe_2O_3 and α-CeO_2 nanocrystals with isometric morphology and an average size of 7 ± 1 and 4 ± 1 nm, respectively. These nanocrystals were found to be evenly distributed and spatially conjugated within the composite.

We believe that, on the basis of their characteristics, the nanocomposites obtained in this work can be used as a basis for highly efficient sorption and catalytic materials, while the proposed approach can provide a foundation for creating new nanostructured substances and composites with crystals sized below 10 nm, high

https://doi.org/10.1016/j.heliyon.2019.e01443

phase homogeneity and uniform distribution of components in the system, which is difficult or impossible to achieve through the use of known methods for their synthesis.

Declarations

Author contribution statement

Vadim Popkov: Conceived and designed the experiments; Performed the experiments; Analyzed and interpreted the data; Contributed reagents, materials, analysis tools or data; Wrote the paper.

Valeri Tolstoy: Conceived and designed the experiments; Analyzed and interpreted the data; Contributed reagents, materials, analysis tools or data; Wrote the paper.

Vladimir Nevedomskiy: Performed the experiments; Analyzed and interpreted the data.

Funding statement

The work was carried out within the framework of the topic "Nanostructured composite materials for catalytic and sorption purification of environmental objects" of the priority direction St. Petersburg State University "Ecology and Rational Nature Management"

Competing interest statement

The authors declare no conflict of interest.

Additional information

No additional information is available for this paper.

Acknowledgements

The work was carried out within the framework of the topic "Nanostructured composite materials for catalytic and sorption purification of environmental objects" of the priority direction St. Petersburg State University "Ecology and Rational Nature Management"

We gratefully acknowledge the «Centre for Optical and Laser Materials Research» of St. Petersburg State University Research park for assistance in the Raman spectroscopy investigations.

https://doi.org/10.1016/j.heliyon.2019.e01443

The PXRD, SEM, EDX and DTA-TG study was performed on the equipment of the engineering center of the Saint-Petersburg State Technological Institute (Technical University).

The TEM-SAED study was performed on the equipment of the Federal Joint Research Centre « Material science and characterization in advanced technology of Ioffe Institute.

References

[1] J. Ameta, A. Kumar, R. Ameta, V.K. Sharma, S.C. Ameta, Synthesis and characterization of $CeFeO_3$ photocatalyst used in photocatalytic bleaching of gentian violet, J. Iran. Chem. Soc. 6 (2009) 293−299.

[2] G.K. Pradhan, K. Parida, Fabrication of iron-cerium mixed oxide: an efficient photocatalyst for dye degradation, Int. J. Eng. Sci. Technol. 2 (2011) 53−65.

[3] D. Ni, Q. Yang, J. Li, J. Ying, C. Tang, P. Tang, Preparation of Ni-doped $CeFeO_3$ by microwave process and its visible-light photocatalytic activity, J. Nanosci. Nanotechnol. 16 (2016) 1046−1049.

[4] H.-X. Wu, T.-J. Wang, X.-M. Dou, B. Zhao, L. Chen, Y. Jin, Spray coating of adsorbent with polymer latex on sand particles for fluoride removal in drinking water, Ind. Eng. Chem. Res. 47 (2008) 4697−4702.

[5] K. Mukhopadhyay, A. Ghosh, S.K. Das, B. Show, P. Sasikumar, U. Chand Ghosh, Synthesis and characterization of cerium(IV)-incorporated hydrous iron(III) oxide as an adsorbent for fluoride removal from water, RSC Adv. 7 (2017) 26037−26051.

[6] Y. Zhang, Preparation and adsorption mechanism of rare earth-doped adsorbent for arsenic (V) removal from groundwater, Sci. China Ser. B. 46 (2003) 252.

[7] Z. He, S. Tian, P. Ning, Adsorption of arsenate and arsenite from aqueous solutions by cerium-loaded cation exchange resin, J. Rare Earths 30 (2012) 563−572.

[8] K. Simeonidis, V. Papadopoulou, S. Tresintsi, E. Kokkinos, I. Katsoyiannis, A. Zouboulis, M. Mitrakas, Efficiency of iron-based oxy-hydroxides in removing antimony from groundwater to levels below the drinking water regulation limits, Sustainability 9 (2017) 238.

[9] F.P.R. Sandra, U.B. Demirci, P. Miele, S. Bernard, Screening and scale-up of cerium oxide-based binary/ternary systems as oxidation catalysts, RSC Adv. 6 (2016) 27426−27433.

https://doi.org/10.1016/j.heliyon.2019.e01443

[10] X. Zhibo, L. Chunmei, G. Dongxu, Z. Xinli, H. Kuihua, Selective catalytic reduction of NO_x with NH_3 over iron-cerium mixed oxide catalyst: catalytic performance and characterization, J. Chem. Technol. Biotechnol. 88 (2013) 1258−1265.

[11] C. Chen, X. Yan, B.A. Yoza, T. Zhou, Y. Li, Y. Zhan, Q. Wang, Q.X. Li, Efficiencies and mechanisms of ZSM5 zeolites loaded with cerium, iron, or manganese oxides for catalytic ozonation of nitrobenzene in water, Sci. Total Environ. 612 (2018) 1424−1432.

[12] X. Zhu, H. Wang, Y. Wei, K. Li, X. Cheng, Hydrogen and syngas production from two-step steam reforming of methane over CeO_2-Fe_2O_3 oxygen carrier, J. Rare Earths 28 (2010) 907−913.

[13] Z. Gu, K. Li, S. Qing, X. Zhu, Y. Wei, Y. Li, H. Wang, Enhanced reducibility and redox stability of Fe_2O_3 in the presence of CeO_2 nanoparticles, RSC Adv. 4 (2014) 47191−47199.

[14] K. Ahn, J.-H. Lee, H. Kim, J. Kim, Enhanced carbon tolerance of Ir alloyed Ni-Based metal for methane partial oxidation, Heliyon 4 (2018), e00652.

[15] V.K. Ivanov, A.B. Shcherbakov, A. V Usatenko, Structure-sensitive properties and biomedical applications of nanodispersed cerium dioxide, Russ. Chem. Rev. 78 (2009) 855−871.

[16] A. Ali, H. Zafar, M. Zia, I. ul Haq, A.R. Phull, J.S. Ali, A. Hussain, Synthesis, characterization, applications, and challenges of iron oxide nanoparticles, Nanotechnol. Sci. Appl. 9 (2016) 49−67.

[17] F. Liu, L. Chen, J.K. Neathery, K. Saito, K. Liu, Cerium oxide promoted iron-based oxygen carrier for chemical looping combustion, Ind. Eng. Chem. Res. 53 (2014) 16341−16348.

[18] H. Liang, Study on the effect of CeO_2 on Fe_2O_3/$LaNiO_3$ as the oxygen carrier applied in chemical-looping hydrogen generation, Int. J. Hydrogen Energy 40 (2015) 13338−13343.

[19] A.H.F. Lee, S.F. Gessert, Y. Chen, N.V. Sergeev, B. Haghiri, Preparation of iron oxide silica particles for Zika viral RNA extraction, Heliyon 4 (2018), e00572.

[20] C. Yadel, A. Michel, S. Casale, J. Fresnais, Hyperthermia efficiency of magnetic nanoparticles in dense aggregates of cerium oxide/iron oxide nanoparticles, Appl. Sci. 8 (2018) 1241.

[21] A.A. Chaugule, H. Kim, Design, synthesis and shape evaluation of cerium iron oxide nanorods for an epoxide opening reaction through azide addition, RSC Adv. 6 (2016) 88859−88867.

 https://doi.org/10.1016/j.heliyon.2019.e01443

[22] B. Chen, Z. Zhu, S. Liu, J. Hong, J. Ma, Y. Qiu, J. Chen, Facile hydrothermal synthesis of nanostructured hollow iron−cerium alkoxides and their superior arsenic adsorption performance, ACS Appl. Mater. Interfaces 6 (2014) 14016−14025.

[23] M.M. Masadeh, G.A. Karasneh, M.A. Al-Akhras, B.A. Albiss, K.M. Aljarah, S.I. Al-azzam, K.H. Alzoubi, Cerium oxide and iron oxide nanoparticles abolish the antibacterial activity of ciprofloxacin against gram positive and gram negative biofilm bacteria, Cytotechnology 67 (2015) 427−435.

[24] E.A. Zaboeva, S.G. Izotova, V.I. Popkov, Glycine-nitrate combustion synthesis of CeFeO3-based nanocrystalline powders, Russ. J. Appl. Chem. 89 (2016) 1228−1236.

[25] V.P. Tolstoy, Successive ionic layer deposition. The use in nanotechnology, Russ. Chem. Rev. 75 (2006) 161−175.

[26] V.P. Tolstoy, The peroxide route of the successive ionic layer deposition procedure for synthesizing nanolayers of metal oxides, hydroxides and peroxides, Thin Solid Films 307 (1997) 10−13.

[27] D.P. Joshi, G. Pant, N. Arora, S. Nainwal, Effect of solvents on morphology, magnetic and dielectric properties of (α-Fe_2O_3@SiO_2) core-shell nanoparticles, Heliyon 3 (2017), e00253.

[28] L.I. Kuklo, V.P. Tolstoy, Successive ionic layer deposition of $Fe_3O_4H_x$-MoO_4nH_2O composite nanolayers and their superparamagnetic properties, Nanosyst. Phys. Chem. Math. 7 (2016) 1050−1054.

[29] A.A. Lobinsky, V.P. Tolstoy, Synthesis of 2D Zn−Co LDH nanosheets by a successive ionic layer deposition method as a material for electrodes of high-performance alkaline battery−supercapacitor hybrid devices, RSC Adv. 8 (2018) 29607−29612.

[30] V.P. Tolstoy, I.A. Kodintsev, K.S. Reshanova, A.A. Lobinsky, A brief review of metal oxide (hydroxide)-graphene nanocomposites synthesis by layer-by-layer deposition from solutions and synthesis of CuO nanorods-graphene nanocomposite, Rev. Adv. Mater. Sci. 49 (2017) 28−37.

[31] J.Z. Marinho, R.H.O. Montes, A.P. de Moura, E. Longo, J.A. Varela, R.A.A. Munoz, R.C. Lima, Rapid preparation of α-FeOOH and α-Fe_2O_3 nanostructures by microwave heating and their application in electrochemical sensors, Mater. Res. Bull. 49 (2014) 572−576.

[32] Y. Wang, M. Liang, J. Fang, J. Fu, X. Chen, Visible-light photo-Fenton oxidation of phenol with rGO-α-FeOOH supported on Al-doped mesoporous silica

https://doi.org/10.1016/j.heliyon.2019.e01443

(MCM-41) at neutral pH: performance and optimization of the catalyst, Chemosphere 182 (2017) 468−476.

[33] J. Gaillard, L. Venault, R. Calvet, S. Del Confetto, N. Clavier, R. Podor, M. Odorico, J.-L. Pellequer, N. Vigier, P. Moisy, Effect of hydration and thermal treatment on ceria surface using non-intrusive techniques, J. Nucl. Mater. 444 (2014) 359−367.

[34] F.H. Scholes, C. Soste, A.E. Hughes, S.G. Hardin, P.R. Curtis, The role of hydrogen peroxide in the deposition of cerium-based conversion coatings, Appl. Surf. Sci. 253 (2006) 1770−1780.

[35] J.F. Perez-Benito, Iron(III)−Hydrogen peroxide reaction: kinetic evidence of a hydroxyl-mediated chain mechanism, J. Phys. Chem. A 108 (2004) 4853−4858.

[36] V. Baldim, F. Bedioui, N. Mignet, I. Margaill, J.-F. Berret, The enzyme-like catalytic activity of cerium oxide nanoparticles and its dependency on Ce^{3+} surface area concentration, Nanoscale 10 (2018) 6971−6980.

[37] G. Gan, P. Zhao, X. Zhang, J. Liu, J. Liu, C. Zhang, X. Hou, Degradation of Pantoprazole in aqueous solution using magnetic nanoscaled Fe_3O_4/CeO_2 composite: effect of system parameters and degradation pathway, J. Alloy. Comp. 725 (2017) 472−483.

[38] J.-S. Lee, S.-C. Choi, Crystallization behavior of nano-ceria powders by hydrothermal synthesis using a mixture of H_2O_2 and NH_4OH, Mater. Lett. 58 (2004) 390−393.

[39] H. Agbe, N. Raza, D. Dodoo-Arhin, A. Chauhan, R.V. Kumar, H_2O_2 rejuvenation-mediated synthesis of stable mixed-morphology Ag_3PO_4 photocatalysts, Heliyon 4 (2018), e00599.

 https://doi.org/10.1016/j.heliyon.2019.e01443